Analyst

RSC Publishing

PAPER

View Article Online
View Journal | View Issue

Cite this: *Analyst*, 2013, **138**, 1249

DNA barcoding *via* counterstaining with AT/GC sensitive ligands in injection-molded all-polymer nanochannel devices

Peter Friis Østergaard,[a] Marco Matteucci,[a] Walter Reisner†[b] and Rafael Taboryski†*[a]

Received 19th October 2012
Accepted 11th December 2012

DOI: 10.1039/c2an36522g

www.rsc.org/analyst

Nanochannel technology, coupled with a suitable DNA labeling chemistry, is a powerful approach for performing high-throughput single-molecule mapping of genomes. Yet so far nanochannel technology has remained inaccessible to the broader research community due to high fabrication cost and/or requirement of specialized facilities/skill-sets. In this article we show that nanochannel-based mapping can be performed in all polymer chips fabricated *via* injection molding: a fabrication process so inexpensive that the devices can be considered disposable. Fluorescent intensity variations can be obtained from molecules extended in the polymer nanochannels *via* chemical counterstaining against YOYO-1. In particular, we demonstrate that the counterstaining induced fluorescent intensity variations to a large degree appear to be proportional to the theoretically computed sequence-maps of both local AT and GC variation along DNA sequences.

1 Introduction

Genomics technology today has two serious drawbacks: (1) extensive fragmentation of the genome is necessitated by sample preparation steps required for currently available sequencing platforms and (2) some form of molecular or clonal amplification is required to produce sufficient sample for analysis. These difficulties tend to increase the complexity of existing platforms, lowering throughput and ultimately increasing cost. For example, the low read lengths of currently available sequencing platforms[1] ensure that the genome assembly and validation, not actual sequencing, is the rate limiting step for de novo analysis of genomes. Moreover, a large portion of the variability in human genomes arises from structural variation[2] (*e.g.* balanced/unbalanced translocations, insertions/deletions, inversions), a large-scale (10 kbp to 1 Mbp) reshuffling of genetic content that can be more difficult to assess from short reads. Critical contextual information, arising from linkage of multiple markers over Mbp-scale genomic regions, is also lost during genomic fragmentation. Amplification steps introduce additional complexity and uncertainty, in particular drop-out of alleles[3] and misrepresentation of certain genomic regions. Finally, there is growing interest in technology platforms with the capability to perform direct genomic analysis at the level of single-cells. Such a capability would preclude the need for cell culture (still relatively time-consuming and laborious) and avoid ensemble averaging over large heterogeneous cellular populations (*e.g.* in a diagnostic situation where sequence information at the single-cell level might be important for optimizing treatment strategies, such as cells obtained from a tumor biopsy).

Nanofluidic devices have the capability of performing analysis at the level of single-molecules, potentially eliminating the need for amplification steps and enabling direct assessment of a biological material in its native state. Nanochannels, constructed with dimensions below the coil-size of typical DNA analytes have the property that they can unscroll individual DNA molecules for linear analysis.[4,5] Parallel nanochannel arrays can be used to isolate and extend many molecules at one time. Continuous throughput is assured by simply driving the molecules through the array *via* either electrophoresis or pressure actuated hydrodynamics, leading to potential throughput ~Gbp per hour. Sequence information is obtained from optical interrogation of the parallel extended molecules *via* a sensitive electron multiplying CCD (EMCCD). Nanochannel technology, despite its advantages, has had limited dissemination into the broader community due to the significant specialized expertise and expense required to produce conventional glass/silicon nanochannel devices. In addition, the cost of the devices tends to limit experimental development of the technique and requires chips to be reused, resulting in nonspecific binding of various compounds to the surface of the chip[6] and cross-contamination issues between experiments.

Specialized labeling strategies are required to read-out sequence maps from the nanochannel extended molecules. One early approach was to perform a restriction digest of a single

[a]*Department of Micro- and Nanotechnology, Technical University of Denmark, DK-2800 Kongens Lyngby, Denmark. E-mail: rata@nanotech.dtu.dk; Tel: +45 4525 8155*

[b]*Department of Physics, McGill University, Montreal, QC, Canada*

† These two authors have shared last authorship.

molecule in a nanochannel.[7] This approach necessarily has the disadvantage that it fragments the analyte during analysis. An alternative enzymatic-based mapping scheme, that does not require DNA fragmentation, is to use a single-stranded nicking enzyme to create a break in one strand (at a particular recognition motif) that is subsequently filled in by DNA polymerase with fluorescent nucleotides.[8–10] These approaches are powerful,[11] but they have the disadvantage of requiring fairly complex and expensive labeling probes or chemistries, and are difficult to implement on-chip, particularly in the context of single-cell analysis. Consequently, there is interest in developing barcoding strategies that are both inexpensive and simple to apply. One recently developed 'non-enzymatic' barcoding strategy is based on a fluorescent analog of denaturation mapping.[12] The principle of this technique is to stain nanochannel extended DNA with a fluorophore (YOYO-1) that unbinds from single-stranded regions. When the molecule is melted *via* a combination of heating and added chemical denaturants, a characteristic pattern of bright and dark bands develops along the molecule containing information on local melting probability (a pattern that can be ultimately related to sequence *via* algorithms that model local chain statistical mechanics). While denaturation mapping has been scaled to enable analysis of intermediate size genomes (such as yeast, ~11 Mbp (ref. 13)), it has a number of drawbacks, in particular the requirement of external heating and the use of toxic reagents such as formamide to ensure denaturation conditions remain in place during an experiment. Such conditions add complexity for any potential commercial realization of the denaturation mapping technique. Moreover, denaturation mapping is naturally limited by fundamental physics to produce banding-patterns that are a function of local melting conditions, with dark-regions of the barcode tending to be AT rich and bright regions GC rich. Recently, Nyberg *et al.*[14] proposed a new type of barcoding technique based on counterstaining the double stranded DNA molecule with netropsin. Netropsin is a minor groove binder with a preference for AT rich regions.[15] The binding of netropsin blocks the binding of uniform DNA stains such as YOYO-1, creating a variation intensity profile that tracks local AT concentration. Since this method does not require partial melting of the DNA, it is not sensitive to the temperature at which the experiment is conducted, eliminating the need for thermal control in the experimental setup and the addition of denaturants to the running buffer.

Here we present a low-cost nanochannel mapping platform based on injection-molded polymer devices.[16,17] Injection-molding is one of the most inexpensive production technologies available (used for example to produce small plastic items used in our everyday life such as tooth-brushes, lego bricks, bottle-caps, *etc.*). Consequently, our injection molded devices have a production cost and time that is significantly lower than that for conventionally nanofabricated silicon and glass devices, so low that these devices can be considered truly disposable. While injection-molded devices have been previously used for extending individual DNA molecules,[18] this publication demonstrates that all-polymer injection-molded devices can be fabricated with a sufficiently low autofluorescence to perform actual DNA sequence mapping. In particular, inspired by chemistries used for counterstaining in classic chromosomal scale karyotyping applications,[19] we demonstrate that the counterstaining approach developed by Nyberg *et al.* can be generalized to include compounds with high GC affinity as well as AT affinity. This generalization of the counter-staining technique allows us to reverse the barcode pattern obtained and enhance the flexibility of the technique to probe sequences with different AT/GC content, a critically important feature due to the large variation of AT/GC content between genomes.

2 Methods and materials

2.1 Chip fabrication

The fluidic chips used for the experiments were fabricated in the cyclic olefin co-polymer TOPAS 5013L-10 (TOPAS Advanced Polymers) *via* injection molding.

To fabricate the chips, a silicon wafer is processed in clean room facilities, using UV-lithography, e-beam-lithography, and reactive ion etching. This gives a silicon wafer with the same topology as the final polymer chips. A 100 nm thick seed layer of nickel vanadium (93% Ni, 7% V) is sputtered on top of the silicon wafer, and a 300 μm thick shim is electroformed on top of the wafer. After separation from the Si wafer, the shim is cut out to fit into a commercial injection molder, enabling mass-production of polymer devices. The reproduced nanochannels at the microchannel inlet are seen in Fig. 1.

After injection molding, the polymer part is bonded with a polymer foil in an UV assisted thermal bonding process,[20] where both foil and chip are exposed for a short time under a UV lamp. The foil and chip are then bonded for 10 min at 115 °C with a pressure of 5 bar. A finished polymer chip is seen in Fig. 2. The dimensions of the nanochannels in these chips are 440 nm wide and 120 nm high. This dimension turned out to ensure the best

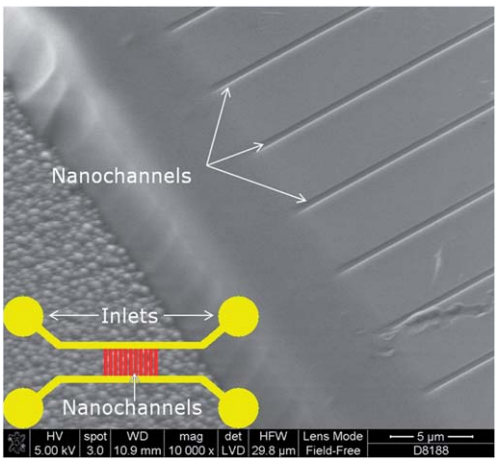

Fig. 1 Scanning electron micrograph of the nanochannels on the injection molded portion of the device. The nanochannels are shown interfaced to the microchannel used for loading polymer solution. The nanochannels have a width of 440 nm and a depth of 120 nm. The sketch at the lower left corner shows the layout of the system.

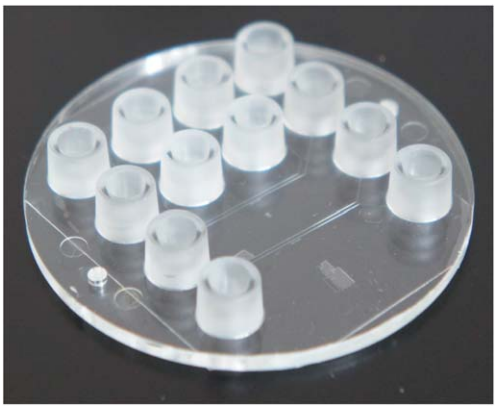

Fig. 2 Injection molded polymer chip. The chip includes ISO-standard Luer fittings for easy access and application of pneumatic pressure. Since a single nanochannel device requires only four inlets, and the chip contains twelve inlets, the design can be iterated three times increasing the multiplexing capability of each chip.

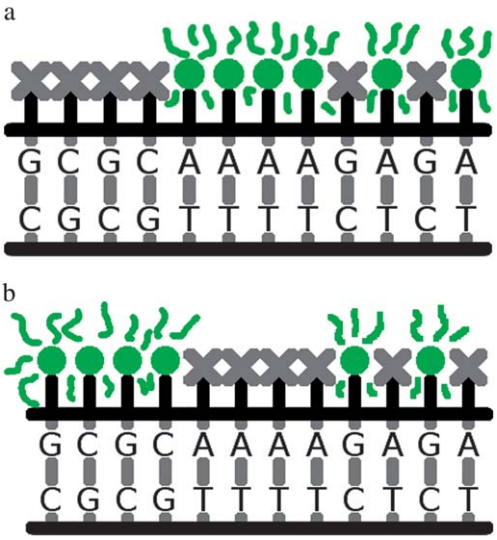

Fig. 3 Principle of the counterstaining approach. The figure on the left corresponds to counterstaining, using actinomycin D, that binds to GC rich regions of the DNA, lowering the degree of binding of YOYO-1 at GC rich regions. The figure on the right corresponds to counterstaining, using netropsin, that binds to AT rich regions of the DNA, lowering the binding of the YOYO-1 at AT rich regions.

trade off between fabrication yield and functionality. The carrier channels leading to the nanochannels are 50 μm wide and 5 μm deep. The fabrication process for producing polymer chips of this kind has been described thoroughly by Tanzi *et al.*[17] These dimensions indicate that we should expect a de Gennes confinement regime[5] rather than the Odijk regime.[21] However, as will be shown, this is sufficient for the experiments performed in this work.

2.2 DNA preparation

Linear λ-DNA (48.5 kbp) and the linear but circularly permuted sequence T4GT7-DNA (168.5 kbp) are used as test constructs to assess the counterstaining technique in injection-molded devices. DNA used in the barcoding experiment is stained with YOYO-1 (Invitrogen), using either netropsin (Sigma-Aldrich) or actinomycin D (Invitrogen) as the counterstaining agent. Netropsin is known to bind to the AT-rich regions of the DNA molecule,[15] limiting the binding of YOYO-1 at this position, while the actinomycin D binds to the GC-rich regions.[22,23] Counterstaining with netropsin will thus result in an inverted fluorescent intensity profile to the one obtained by counterstaining with actinomycin D. The principle behind the counterstaining is presented graphically in Fig. 3.

For 100 μL of stained DNA, counterstained with actinomycin D, 1 μg of DNA is mixed with actinomycin D and YOYO-1. The ratio of base pairs to YOYO-1 molecules is 10 : 1 and the ratio of actinomycin D molecules to YOYO-1 molecules is 250 : 1. The suspension is incubated for 2 h at 50 °C, and stored at −20 °C until use. The best results are obtained if experiments are performed shortly after staining of the DNA. Counterstaining with netropsin is performed exactly as described above, only exchanging the actinomycin D with netropsin in a concentration that is 4000 times higher than the concentration of YOYO-1.

2.3 Experimental setup

The polymer chips are initially pre-wetted with a 7% ethanol solution which is exchanged with 0.5× Tris/Borate/EDTA (TBE) prior to introduction of DNA. The counterstained and YOYO-1 labelled DNA solution is then diluted 1 : 10 in degassed 0.5× TBE. Triton X-100 (Sigma-Aldrich) is added at 0.5% (v/v) to the loading buffer to prevent sticking of the DNA to the polymer surface. In addition, 0.5× TBE containing 3% (v/v) β-mercaptoethanol (Sigma-Aldrich) is added to avoid photonicking. The DNA solution is then introduced into one of the luer ports on the device and the ports are connected to an air-pump for applying positive pressure. DNA molecules are brought from the luer reservoir to the nanochannel inlet by applying the pressure drop across the microchannel. Subsequently, the flow can be redirected to drive DNA into the nanochannel array by applying pressure across the nanochannels. As the DNA enters the nanochannel, the channel confinement forces the DNA to stretch out to around 25% of its contour length, in good agreement with previously published simulated data.[21] The dimensions of the channels correspond to the DNA being in the de Gennes regime, as described by Reisner *et al.*[5] and Brochard and de Gennes,[24] and while a more profound stretching would be beneficial for the resolution of the data,[25,26] it was still possible to get a high confidence of the results obtained during the experiments. The fluorescence profile across the nanochannel DNA contains sequence information with a resolution limited by optical diffraction and the degree of stretching to around 2 kbp. Raw images of λ-DNA inside the nanochannels are shown in Fig. 4. Data acquisition is performed using an inverted Nikon microscope (Nikon Eclipse Ti) with a 100× oil immersion objective (NA = 1.4) and an EMCCD (Andor). Molecules are imaged for 50 consecutive images with a frame rate of 10 fps.

During the time used for an experiment, neither significant photonicking nor photobleaching was experienced.

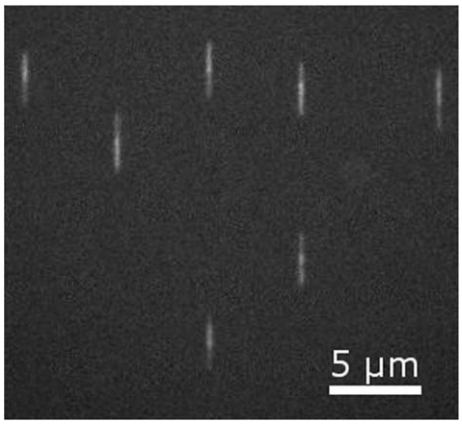

Fig. 4 λ-DNA inside the nanochannels. The physical confinement of the nanochannels forces the DNA molecules to stretch out.

3 Results and discussion

3.1 Barcoding

The goal of our analysis procedure is to extract a high-signal to noise barcode from the raw single-molecule data. To obtain this goal, it is important, that the autofluorescence of the polymer chip is as low as possible. The TOPAS COC is known for having a small change in autofluorescence over time,[27,28] along with an initially low autofluorescence value. In our setup, the average measured background signal measured over the entire field of view, was only 1.6 ± 0.3 times higher than that of a similar chip, fabricated in fused silica, excited with light having a wavelength of 480 nm and data recorded at 535 nm (a method proposed by S. Stavis[29]). Four measurements were performed on both polymer and glass chips to obtain the quoted standard deviation.

The intensity profile transverse to the axis of stretching contains information only about the optical resolution. Consequently, for a given molecule, we sum the intensity transverse to the nanochannel axis and plot this intensity along the nanochannel, converting the image stack to a gray scale plot of intensity *vs.* the position along the channel on one axis and time on the other axis. In order to average intensity profiles captured at different times we must take into account thermal (Brownian) fluctuations of the molecule that induce distortions of the barcode between frames. Brownian dynamics create displacements of the center-of-mass position *via* diffusion and fluctuations in local molecule concentration (arising as a superposition of spatial Fourier modes along the extended molecule). Thermal fluctuations are taken into account *via* the approach described by Reisner *et al.*[12] Center-of-mass motion of DNA is removed *via* direct calculation of molecule spatial translation (obtained from correlation of intensity profiles between frames). Concentration fluctuations are removed by computing the series of local dilations that minimize the least squared difference between a reference frame (taken as the initial frame) and a given frame in the image series. If this procedure is applied to all frames acquired, the intensity profile between frames will be normalized and can be averaged together, yielding a single-molecule barcode with the highest signal-to-noise possible for the given dataset. For each set of parameters used, at least 30 molecules are measured, so that it is possible to obtain average barcodes that represent the consensus of a number of single-molecule measurements.

We expect intensity variation arising from counterstaining to be a function of the local AT/GC concentration. In particular, we expect the local intensity $I(s)$ as a function of sequence position s along the nanochannel extended molecule to be proportional to the local GC concentration (for netropsin) and AT concentration (actinomycin D) with a proportionality factor that depends on the level of YOYO-1 staining. The local AT/GC concentration is obtained convolving a binary version of the genetic code, where ATs and GCs are converted into either ones or zeros, depending on whether netropsin or actinomycin is used, with a Gaussian profile having a standard deviation of 1.5 pixels/200 nm to simulate broadening due to finite optical resolution.

The experimentally obtained barcode is normalized using the algorithm

$$P_{\text{exp}} = \frac{I_{\text{exp}} - \langle I_{\text{exp}} \rangle}{\sqrt{\left\langle \left(I_{\text{exp}} - \langle I_{\text{exp}} \rangle \right)^2 \right\rangle}}$$

where I_{exp} is the EMCCD camera pixel value reading.

The normalized barcodes were aligned to the theoretical profile, after normalization of the theoretical barcode, the same way as for the experimental one.

$$P_{\text{theory}} = \frac{I_{\text{theory}} - \langle I_{\text{theory}} \rangle}{\sqrt{\left\langle \left(I_{\text{theory}} - \langle I_{\text{theory}} \rangle \right)^2 \right\rangle}}$$

Inter-profile shift that yields a minimum of the squared intensity difference between the profiles (summed across all pixels), was then found, *i.e.* we find the least squares estimator for barcode no. i as

$$\delta_i = \min \sum_{n=s}^{m+s} \frac{\left(P_{\text{exp},i}(n) - P_{\text{theory}}(n) \right)^2}{m}$$

where s is the starting point along the theoretical barcode that is used as an optimizing parameter, and m is the pixel length of the barcode.

During this alignment process we also dilated or contracted the theoretical barcode by up to 15% to yield the best fit (this procedure takes into account the fact that the measured barcode may not exactly represent the true equilibrium profile). In addition, for the linear λ-DNA sequence we must find the reading direction of the molecule that yields the best alignment, while alignment of the circularly permuted T4GT7-DNA sequence also requires determination of the sequence-starting point. The average of the fitted barcodes, $P_{\text{consensus}} = \langle \delta_i \rangle$, from the DNA used in the experiments is shown in Fig. 5. The expected inversion of the barcodes, occurring as an effect of changing the counterstaining agent from actinomycin D to netropsin, is easily seen, when comparing the figures to the left of Fig. 5 to the figure to the right.

Although it is shown, that there is a clear correspondence between the measured intensity and the level of AT/GC content in the molecule, the difference in exposure over the field of view of the microscope makes it challenging to directly translate a measured intensity profile to an AT/GC content of a molecule. However, we can always normalize to the intensity variation caused by non-uniform illumination by analysis of how the background levels vary. This normalization was not necessary for the relatively short molecules used in these experiments as the region of interest was small enough for the background to be constant within the region. Hence if part of the molecule is known and can be used as reference, the AT/GC level of the rest of the molecule can also be measured.

3.2 Validity of fit

To ensure that the fit to the theoretical barcode is not just a fit based on random noise in the system, but a fit to the underlying DNA sequence, the experimental profile is also aligned to 500 randomly generated barcodes, giving 500 consensus barcodes, using the same procedure as the alignments to the true theoretical barcode. In order to measure the goodness of fit, we will define an estimator that is the standard deviation between the average experimental barcode and the theoretical barcode.

$$\sigma_j = \sqrt{\left\langle \left(\Delta P_j - \langle \Delta P_j \rangle\right)^2 \right\rangle}$$

ΔP being the difference between the consensus barcode, and its corresponding, randomly generated, theoretical barcode.

In the case of T4GT7 DNA stained with actinomycin D, estimator values for all 500 random barcodes are histogramed and are seen to follow a near perfect Gaussian distribution with a mean of 0.742 and standard deviation of 0.086 as seen in Fig. 6. We observe that the estimator value found when aligning the experimental barcodes to the real theoretical barcode is far away from the centre of this distribution, so that it has a very low probability of happening by chance (we find the probability that an alignment of this quality would happen by chance is 1.9×10^{-7}). However, even though there is a clear correspondence between the data and the theory in Fig. 5, some deviations are observed, *e.g.* peaks between 30 and 50 kbp are not present in the data at the top right graph. We believe these deviations most probably should be explained by shortcomings of the simple theoretical model applied here. As previously described by Nyberg *et al.*,[14] the large peaks in the intensity map are easily seen when comparing the experimental data with the theoretical curve, but the small features are blurred out due to thermal fluctuation and diffusion.

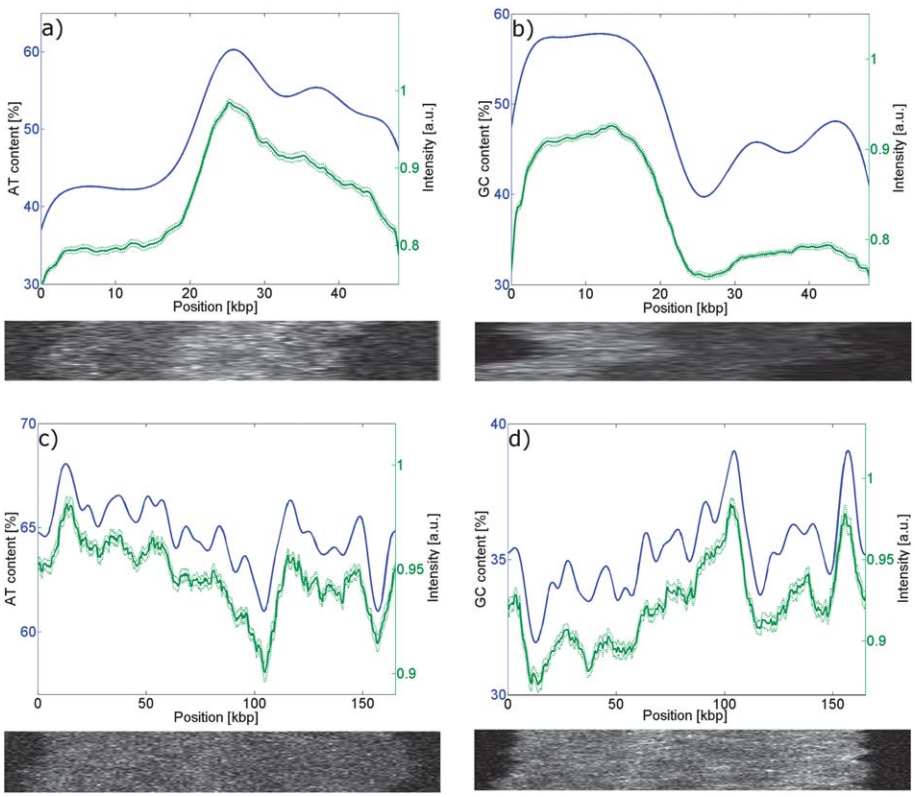

Fig. 5 Theoretical and experimental barcodes for the DNA sequences used in the experiments. (a) is λ-DNA counter stained with actinomycin D, (b) is λ-DNA counterstained with netropsin, (c) is T4GT7-DNA counter stained with actinomycin D, and (d) is T4GT7-DNA counter stained with netropsin. In all cases, the blue line uses the *y*-axis on the left, and corresponds to the theoretical barcode, while the green line uses the *y*-axis on the right, and corresponds to the average experimental barcode. The dotted green lines indicate the standard deviation of the average barcode. Below each barcode is seen a recording of a single molecule, measured for that specific experiment. At least 30 molecules were used in order to get the average experimental barcode and the corresponding confidence limits.

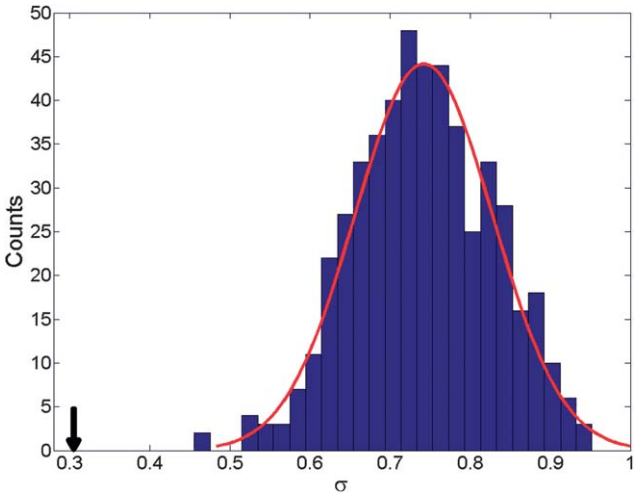

Fig. 6 Distribution of estimator values σ obtained by comparing experimental barcode for T4GT7 counter stained with actinomycin D against random barcodes. The dark arrow indicates the estimator value obtained from the fit against a theoretical barcode determined from the known sequence. This estimator value is sufficiently low that we would not expect it to occur by chance.

4 Conclusion

In conclusion we have demonstrated a proof of concept that direct barcoding using counterstaining against YOYO-1 with either GC or AT selective ligands can facilitate fast identification of specific DNA samples. We have also demonstrated that this barcoding can be performed *via* disposable injection molded devices, a feature which may facilitate future adoption of this technology. We emphasize that the possibility of mapping chemistries that can probe either GC or AT content is highly advantageous, as it allows selection of the mapping chemistry that gives the highest signal contrast possible for a given sequence region. For example, if a sequence loci under investigation is known to have a large GC concentration, it would be beneficial to use netropsin, since this will still leave the GC sites mostly free and YOYO-1 will bind to the residual regions of high AT concentration. The same is true for sequences having a large AT content, where it would be beneficial to use actinomycin D. Along with the use of cheap, disposable polymer chips, this counterstaining technique has potential of reducing the cost of performing genetic barcoding, as – with the single exception of YOYO-1 – it does not require any expensive fluorescent probes or reagents.

Acknowledgements

The authors gratefully acknowledge funding from the Danish Council for Strategic Research, DSF, under the grant agreement no. 10-092322 (PolyNano). The authors would like to thank Henrik Flyvbjerg, Rodolph Marie, and Rob Welch for fruitful discussions, and the staff of DTU DANCHIP for practical help with the device fabrication.

References

1 J. Shendure and H. Ji, *Nat. Biotechnol.*, 2008, **26**, 1135–1145.
2 J. M. Kidd, G. M. Cooper, W. Donahue, H. Hayden, N. Sampas, T. Graves, N. Hansen, B. Teague, C. Alkan, F. Antonacci, E. Haugen, T. Zerr, N. Yamada, P. Tsang, T. Newman, E. Tuzun, Z. Cheng, H. Ebling, N. Tusneem, R. David, W. Gillett, K. Phelps, M. Weaver, D. Saranga, A. Brand, W. Tao, E. Gustafson, K. McKernan, L. Chen, M. Malig, J. Smith, J. Korn, S. McCarroll, D. Altshuler, D. Peiffer, M. Dorschner, J. Stamatoyannopoulos, D. Schwartz, D. Nickerson, J. Mullikin, R. Wilson, L. Bruhn, M. Olson, R. Kaul, D. Smith and E. Eichler, *Nature*, 2008, **453**, 56–64.
3 W. Piyamongkol, M. G. Bermudez, J. C. Harper and D. Wells, *Hum. Mol. Genet.*, 2003, **9**, 411–420.
4 J. Tegenfeldt, C. Prinz, H. Cao, S. Chou, W. Reisner, R. Riehn, Y. Wang, E. Cox, J. Sturm, P. Silberzan and R. Austin, *Proc. Natl. Acad. Sci. U. S. A.*, 2004, **101**, 10979–10983.
5 W. Reisner, K. Morton, R. Riehn, Y. Wang, Z. Yu, M. Rosen, J. Sturm, S. Chou, E. Frey and R. Austin, *Phys. Rev. Lett.*, 2005, **94**, 196101.
6 D. Huber, R. Manginell, M. Samara, B. Kim and B. Bunker, *Science*, 2003, **301**, 352–354.
7 R. Riehn, M. C. Lu, Y. M. Wang, S. F. Lim, E. C. Cox and R. H. Austin, *Proc. Natl. Acad. Sci. U. S. A.*, 2005, **102**, 10012–10016.
8 K. Jo, D. M. Dhingra, T. Odijk, J. J. de Pablo, M. D. Graham, R. Runnheim, D. Forrest and D. C. Schwartz, *Proc. Natl. Acad. Sci. U. S. A.*, 2007, **104**, 2673–2678.
9 M. Xiao, A. Phong, C. Ha, T.-F. Chan, D. Cai, L. Leung, E. Wan, A. L. Kistler, J. L. DeRisi, P. R. Selvin and P.-Y. Kwok, *Nucleic Acids Res.*, 2007, **35**, e16.
10 S. K. Das, M. D. Austin, M. C. Akana, P. Deshpande, H. Cao and M. Xiao, *Nucleic Acids Res.*, 2010, **38**, e177.
11 E. Lam, A. Hastie, C. Lin, D. Ehrlich, S. Das, M. Austin, P. Deshpande, H. Cao, N. Nagarajan, M. Xiao and P.-Y. Kwok, *Nat. Biotechnol.*, 2012, **30**, 771–776.
12 W. Reisner, N. B. Larsen, A. Silahtaroglu, A. Kristensen, N. Tommerup, J. O. Tegenfeldt and H. Flyvbjerg, *Proc. Natl. Acad. Sci. U. S. A.*, 2010, **107**, 13294–13299.
13 R. L. Welch, R. Sladek, K. Dewar and W. Reisner, *Lab Chip*, 2012, **12**, 3314–3321.
14 L. K. Nyberg, F. Persson, J. Berg, J. Bergstrom, E. Fransson, L. Olsson, M. Persson, A. Stalnacke, J. Wigenius, J. O. Tegenfeldt and F. Westerlund, *Biochem. Biophys. Res. Commun.*, 2012, **417**, 404–408.
15 R. Wartell, J. Larson and R. Wells, *J. Biol. Chem.*, 1974, **249**, 6719–6731.
16 K. O. Andresen, M. Hansen, M. Matschuk, S. T. Jepsen, H. S. Sorensen, P. Utko, D. Selmeczi, T. S. Hansen, N. B. Larsen, N. Rozlosnik and R. Taboryski, *J. Micromech. Microeng.*, 2010, **20**, 055010.
17 S. Tanzi, P. F. Østergaard, M. Matteucci, T. L. Christiansen, J. Cech, R. Marie and R. Taboryski, *J. Micromech. Microeng.*, 2012, **22**, 115008 (11pp.).
18 P. Utko, F. Persson, A. Kristensen and N. B. Larsen, *Lab Chip*, 2011, **11**, 303–308.
19 D. Schweizer, *Hum. Genet.*, 1981, **57**, 1–14.
20 M. Matteucci, T. L. Christiansen, S. Tanzi, P. F. Østergaard and R. Taboryski, Presented at the 38th International

Conference on Micro and Nano Engineering, September 16–20, 2012, Toulouse, France, 2012, submitted.
21 Y. Wang, D. R. Tree and K. D. Dorfman, *Macromolecules*, 2011, **44**, 6594–6604.
22 E. Scott, R. Jones, D. Banville, G. Zon, L. Marzilli and W. Wilson, *Biochemistry*, 1988, **27**, 915–923.
23 W. Wilson, R. Jones, G. Zon, E. Scott and L. Marzilli, *Biophys. J.*, 1988, **53**, A4.
24 F. Brochard and P. de Gennes, *J. Chem. Phys.*, 1977, **67**, 52–56.
25 Y. Wang, W. F. Reinhart and D. R. Tree, *Biomicrofluidics*, 2012, **6**, 014101.
26 Y. Kim, K. S. Kim, K. L. Kounovsky, R. Chang, G. Y. Jung, J. J. de Pablo, K. Jo and D. C. Schwartz, *Lab Chip*, 2011, **11**, 1721–1729.
27 K. R. Hawkins and P. Yager, *Lab Chip*, 2003, **3**, 248–252.
28 A. Piruska, I. Nikcevic, S. H. Lee, C. Ahn, W. R. Heineman, P. A. Limbach and C. J. Seliskar, *Lab Chip*, 2005, **5**, 1348–1354.
29 S. M. Stavis, *Lab Chip*, 2012, **12**, 3008–3011.